Interaction and Multiscale Mechanics, *Vol. 6, No. 2 (2013) 173-195*
DOI:http://dx.doi.org/10.12989/imm.2013.6.2.173

Concrete fragmentation modeling using coupled finite element - meshfree formulations

Youcai Wu*, Hyung-Jin Choi and John E. Crawford

Karagozian & Case (K&C), 700 N. Brand Blvd., Suite 700, Glendale, CA 91203, USA

(Received March 3, 2013, Revised April 10, 2013 Accepted May 7, 2013)

Abstract. Meshfree methods are known to have the capability to overcome the strict regularization requirements and numerical instabilities that encumber the finite element method (FEM) in large deformation problems. They are also more naturally suited for problems involving material perforation and fragmentation. To take advantage of the high efficiency of FEM and high accuracy of meshfree methods, a coupled finite element (FE) and reproducing kernel (RK, one of the meshfree approximations) formulation is described in this paper. The coupling of FE and RK approximation is implemented in an evolutionary fashion, where the extent and location of the evolution is dependent on a triggering criteria provided by the material constitutive laws. To enhance computational efficiency, Gauss quadrature is applied to integrate both FE and RK domains so that no state variable transfer is required when mesh conversion is performed. To control the hourglassing that might occur with 1-point integrated hexahedral grids, viscous type hourglass control is implemented. Meanwhile, the FEM version of the K&C concrete (KCC) model was modified to make it applicable in both FE and RK formulations. Results using this code and the KCC model are shown for the modeling of concrete responses under quasi-static, blast and impact loadings. These analyses demonstrate that fragmentation phenomena of the sort commonly observed under blast and impact loadings of concrete structures was able to be realistically captured by the coupled formulation.

Keywords: Reproducing Kernel (RK); Finite Element (FE); coupled FE/RK; fragmentation; concrete

1. Introduction

Since its origination (Courant 1942), the finite element method (FEM) has been widely documented in the literature and a number of implicit and explicit FEM solvers, such as ANSYS, LS-DYNA, DYNA3D and ADINA, have been developed. The discretization of the problem domain in FEM is achieved by using elements, typically with very simple shape functions and high order quadrature rules. FEM has been proved itself to be a robust analysis method for numerous varieties of engineering and scientific problems. However, in applications, FEM is known to have difficulties with problems involving large deformations and moving discontinuities, such as the extremely large deformations incurred in some manufacturing processes, or the growth of cracks with arbitrary and complex paths present in failure (fragmentation) processes. For these kinds of problems, the finite element solution is highly mesh-dependent.

*Corresponding author, Professor, E-mail: wu@kcse.com

http://www.techno-press.org/?journal=imm&subpage=7 ISSN: 1976-0426 (Print), 2092-6200 (Online)

Meshfree methods, on the other hand, discretize the problem domain by a set of particles or nodes, which are not connected to form any sort of mesh or element. The meshfree approximation is performed completely in terms of these discrete particles and the meshfree shape functions associated with each particle exhibit a compact support (i.e., cover only a small portion of the domain). Thus, it has become possible to solve many types of problems that are difficult to handle with mesh-based methods (e.g., FEM) and avoid the regularity requirements caused by the mesh needed by these methods. Well known meshfree methods include the smoothed particle hydrodynamics (SPH) (Gingold and Monaghan 1977 and Monaghan 1988), the element-free Galerkin (EFG) (Belytschko *et al.* 1994, 1995), the material point method (MPM) (Bardenhagen and Kober 2004) and the reproducing kernel particle method (RKPM) (Liu *et al*. 1995, Chen *et al.* 1996).

The shape functions of the RKPM (Liu *et al.* 1995, Chen *et al.* 1996) are constructed solely based on the positions of the discrete particles used in discretizing the problem domain while no connectivity information is involved. The solution accuracy of this type of approximation has no strong dependence on domain discretization and there are no mesh distortion issues, which appear frequently in element based methods such as FEM for large deformation problems. Therefore, large deformation problems can be solved by the RKPM with a Lagrangian formulation (Chen *et al.* 1996). The Lagrangian RKPM has been applied in many solid mechanics problems such as rubber (Chen *et al.* 1998b), metal forming (Chen *et al.* 1998a) and geotechnical materials (Chen *et al.* 2001b, Wang *et al.* 2011) and even computational fluid dynamics (Liu *et al.* 1997).

However, similar to FEM, the Lagrangian RKPM has some regularization requirements as well and was found ineffective for modeling extremely large deformation problems, such as earth bulldozing problems (Wu 2005). This is because the deformation gradient, which is required for mapping the current configuration and the reference configuration, loses positive definiteness and cannot provide a one-to-one mapping at some material points. Therefore, a semi-Lagrangian reproducing kernel approximation was developed (Wu 2005, Chen and Wu 2007). In the semi-Lagrangian formulation, the kernel function and its support are evaluated in the current configuration and all approximations are performed in this configuration, therefore, the deformation gradient is not required any more. The spatial and temporal stability of the semi-Lagrangian approach was established by Chen and Wu (2007) and Guan *et al.* (2009). Physical responses were obtained in the analyses of earth bulldozing (Guan *et al.* 2009) and high velocity fragment-impact problems (Guan *et al.* 2011, Wu *et al.* 2013) with the semi-Lagrangian formulation.

There are two ways to integrate the RKPM weak form formulations. One is the traditional Gauss integration. With high order Gauss quadrature rules, RKPM formulations are able to effectively solve many solid mechanics problems (Chen *et al.* 1996, 1998a, 1998b and 2001b). However, Gauss integration was shown not to satisfy integration constraints (Chen *et al.* 2001a), which are essential for obtaining optimum convergence rates and accuracy. Therefore, a stabilized conforming nodal integration (SCNI) technique was developed by Chen *et al.* (2001a, 2002) to remedy this shortcoming. Unlike Gauss integration, which needs background grids, SCNI performs integration directly at nodal points. Thus, both its efficiency (convergence rate) and accuracy are high. The SCNI technique was also generalized to beam, plate and shell formulations by Wang and Chen (2004, 2006, 2008), Chen and Wang (2006), Wang and Wu (2008), Wang and Sun (2011) and Wang and Lin (2011).

In this research, a coupled finite element – reproducing kernel (FE/RK) scheme is implemented into the DYNA3D code (Lin 2005) for modeling concrete fragmentation behaviors through the

post-failure regime. The primary objective of this coupling approach is to provide a more effective and accurate means to capture responses in highly distorted and damaged regions of the model (by RKPM), which may involve regions where the formation of shear band localization is occurring, cratering and ejecta caused by fragment impacts is of interest and other complex behaviors which are difficult for FEM. The weak form of the coupled formulation is integrated by Gauss integration. Viscous type hourglass control (Flanagan and Belytschko, 1981) is implemented to suppress hourglass modes when one-point quadrature rule is applied for hexahedral integration grids.

To enable the coupled FEM/RKPM scheme to model concrete behaviors physically, the K&C concrete (KCC) model (Malvar *et al.* 1997) was extended to work with the meshfree discretization. The internal damage variable of the KCC model was selected as the criteria for triggering the conversion (evolution) from FE approximation to RK approximation. Compared with other approaches such SPH (Rabczuk and Eibl 2003) in modeling concrete fragmentation, this evolutionary coupling approach allows for only those parts of the FEM mesh that are badly distorted to be converted, which afforded an overall faster solution since meshfree solvers are much slower. Meanwhile, the concrete constitutive law employed in this study is widely accepted. Results from several analyses are presented to demonstrate the application of the coupled formulations, including concrete results for quasi-static responses and fragmentation responses induced by blast and impact loads.

The organization of this paper is: Section 2 describes the coupled formulations; Section 3 briefly introduces the K&C concrete (KCC) model; Section 4 presents the numerical applications of the coupled schemes; and the last section concludes the current study.

2. Coupled finite element / reproducing kernel approximation

Due to its simple shape functions (usually, piece-wise linear), the FEM has high efficiency but low accuracy (because of low order shape functions). On the other hand, due to its high order consistency, the RKPM has high accuracy but low efficiency (to deal with high order shape functions). To take advantage of both FE and RK formulations (i.e., high efficiency of FEM and high accuracy of RKPM), several methods were developed and evaluated for coupling FEM and RKPM discretizations, which are discussed by Guo *et al.* (2004), Crawford *et al.* (2005), Chen *et al.* (2006), Wang *et al.* (2009) and Wu *et al.* (2013). In this research, a coupled FE and RK technique is implemented under the DYNA3D (Lin 2005) framework to model concrete fragmentation processes by discretizing the highly damaged regions with RKPM and other regions with FEM. Therefore, better accuracy (than pure FEM) and higher efficiency (than pure RKPM) are obtained.

Gauss integration, which is widely applied in many FEM codes, is employed in the domain integration in DYNA3D. Satisfactory accuracy is achieved even with low order quadrature rules (such as one-point integration) in explicit calculations, which is very efficient. Therefore, to assure the efficiency of the coupled simulation, Gauss integration is also applied to integrate RKPM domains and the integration cells for the RKPM domains are exactly the same elements used in finite element discretization. By doing so, state variable transition is not required when the FEM domain is converted to an RKPM domain since the state variables are stored at the same integration points before and after conversion. In addition, a minor advantage of Gauss integration over nodal based integration (e.g., SCNI or direct nodal integration) is that no special treatment is needed for the stiffness of interface nodes between various materials since the stiffness is

evaluated at integration points rather than nodal points in Gauss integration while each integration cell belongs to only one material. On the other hand, the stiffness of interface nodes between various materials needs to be approximated by such means as interpolation or averaging in a nodal based integration.

2.1 Coupling scheme

The coupled simulation starts with FEM for the entire domain and then the FEM nodes are dynamically converted to RKPM nodes based on a user defined triggering mechanism (explained later). Since the same quadrature rule (Gauss) is applied for both FEM and RKPM domains, the FEM – RKPM conversion is performed directly (i.e., the only change being the use of the RK shape function to replace the FE shape function when the conversion is carried out). Therefore, the FE and RK shape functions are first constructed at all the integration points respectively and then they are coupled according to

$$\tilde{\Psi}_I(\mathbf{x}) = (1-R)N_I(\mathbf{x}) + R\Psi_I(\mathbf{x}) \tag{1}$$

where $\tilde{\Psi}_I(\mathbf{x})$ is the coupled shape function of node I evaluated at integration point $\mathbf{x}$; $N_I(\mathbf{x})$ is the standard FE shape function; $\Psi_I(\mathbf{x})$ is the RK shape function (introduced in the next sub-section); $R\,(0 \le R \le 1)$ is the coupling function. The coupled shape function $\tilde{\Psi}_I(\mathbf{x})$ satisfies partition of unity automatically since the FE and RK shape functions satisfy partition of unity respectively.

The scheme for the coupling is graphically illustrated in Fig. 1. The coupling function R starts with zero for all integration points so that the whole domain is approximated by FE formulation. When the triggering criteria is satisfied, R is set to unity at the specific integration point and the coupled shape function is defined according to Eq. (1). For example, when the damage at integration point $\mathbf{x}_0$ (i.e., at the center of the integration cell or element if one-point integration is used) satisfies the triggering criteria, R at $\mathbf{x}_0$ is set to unity and then: the nodes within the region covered by the sphere (or a circle in two dimensions) with radius of d_1 (usually d_1 is bigger than the maximum support size of all the nodes in the specific element) are converted to RKPM nodes; the nodes outside the region covered by the sphere of d_2 are kept as FEM nodes; and the nodes between the two spheres with radii of d_1 and d_2 are defined as coupled FEM/RKPM nodes with $R = (d_2 - d)/(d_2 - d_1)$, where d is the distance to point $\mathbf{x}_0$ and the coupled shape functions are constructed for these nodes according to Eq. (1). The linear variation of R ensures the transition between FE approximation and RK approximation to be smooth.

2.2 Lagrangian reproducing kernel shape function

The Lagrangian finite element (FE) approximation of an arbitrary function $u(\mathbf{X})$, denoted by $u^h(\mathbf{X})$, can be written as

$$u^h(\mathbf{X}) = \sum_{I=1}^{NEM} N_I(\mathbf{X}) u_I \tag{2}$$

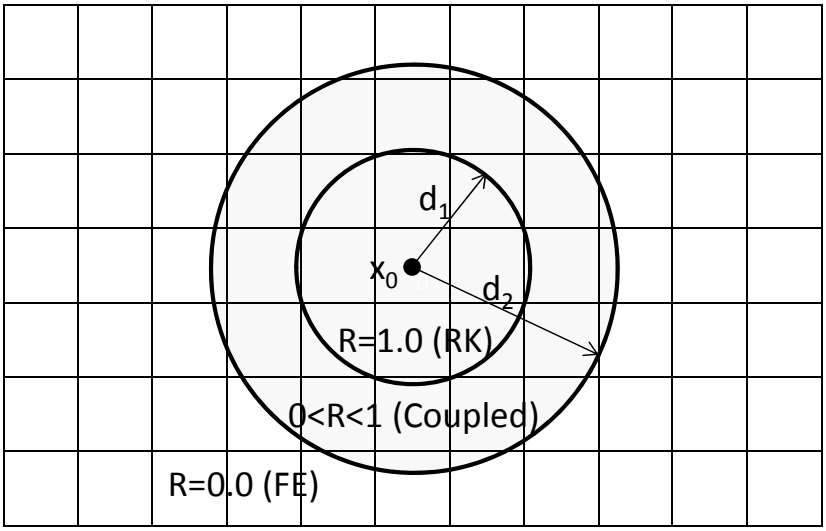

Fig. 1 FE/RK coupling scheme

where $N_I(\mathbf{X})$ is the finite element (FE) shape function of node I evaluated at point $\mathbf{X}$, u_I is the coefficient of the approximation at node I and NEM is the number of nodes in the element.

Similar to the FE approximation, the Lagrangian reproducing kernel (RK) approximation of an arbitrary function $u(\mathbf{X})$, can be expressed as

$$u^h(\mathbf{X}) = \sum_{I=1}^{NP} \Psi_I(\mathbf{X}) d_I \tag{3}$$

where NP is the number of particles that are employed in the discretization of the problem domain, d_I is the coefficient of the approximation at node I and $\Psi_I(\mathbf{X})$ is the RK shape function evaluated at point $\mathbf{X}$. The RK shape function is constructed by a multiplication of the correction function and the kernel function as follows (Liu *et al.* 1995 and Chen *et al.* 1996)

$$\Psi_I(\mathbf{X}) = C(\mathbf{X};\mathbf{X}-\mathbf{X}_I)\Phi_a(\mathbf{X}-\mathbf{X}_I) \tag{4}$$

where $\Phi_a(\mathbf{X}-\mathbf{X}_I)$ is the kernel function that defines the smoothness and locality of the approximation with a compact support Ω_I (see Fig. 2) measured by a. A commonly used kernel function is the cubic B-spline function (Eq. (5)), which gives C^2 continuity (smoothness).

$$\Phi_a(\mathbf{X}-\mathbf{X}_I) = \begin{cases} 2/3 - 4z^2 + 4z^3 & for \quad z \le 1/2 \\ 4/3 - 4z + 4z^2 - 4/3z^3 & for \quad 1/2 < z \le 1 \\ 0 & for \quad z > 1 \end{cases} \qquad z = |\mathbf{X}-\mathbf{X}_I|/a \tag{5}$$

The compact support a defines the unique small region (or, the so-called domain of influence -DOI) pertaining to node K where its shape function is non-zero. The union of all the kernel

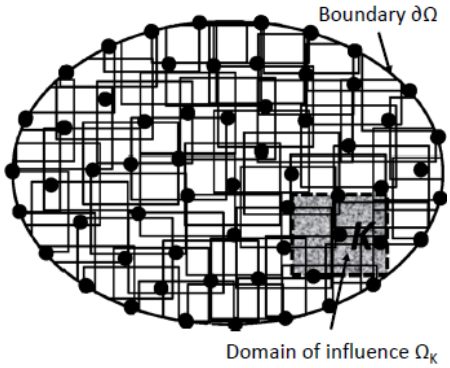

Fig. 2 Meshfree domain discretization and domain of influence

supports should cover the entire problem domain (i.e., $\bigcup_K \Omega_K \supset \Omega$ as shown in Fig. 2). Each black dot in Fig. 2 represents a node and the rectangle (brick in three-dimension) centered at the node denotes its support. The kernel support is truncated at the geometric boundary of the problem domain. The support size a must be big enough so that the DOIs overlap each other and every point in the whole domain is covered by a sufficient number of kernels to ensure that the moment matrix (expressed later in Eq. (11)) is invertible.

The term $C(\mathbf{X};\mathbf{X}-\mathbf{X}_I)$ in Eq. (4) is often called the correction function (Chen *et al.* 1996). This function determines the completeness and consistency of the meshfree approximation. The correction function $C(\mathbf{X};\mathbf{X}-\mathbf{X}_I)$ is usually constructed from a linear combination of monomials (Liu *et al*. 1995)

$$C(\mathbf{X};\mathbf{X}-\mathbf{X}_I)=\sum_{i+j+k=0}^{n}(X_1-X_{1I})^i(X_2-X_{2I})^j(X_3-X_{3I})^k b_{ijk}(\mathbf{X})=\mathbf{H}^T(\mathbf{X}-\mathbf{X}_I)\mathbf{b}(\mathbf{X}) \qquad i,j,k\geq 0 \tag{6}$$

with the basis function $\mathbf{H}(\mathbf{X}-\mathbf{X}_I)$ being defined as

$$\mathbf{H}^T(\mathbf{X}-\mathbf{X}_I)=\begin{bmatrix}1 & X_1-X_{1I} & X_2-X_{2I} & \cdots & (X_3-X_{3I})^n\end{bmatrix} \tag{7}$$

$$\mathbf{b}(\mathbf{X})=\begin{bmatrix}b_{000} & b_{100} & b_{010} & \cdots & b_{00n}\end{bmatrix} \tag{8}$$

where n is the order of the complete monomial basis, which also defines the completeness of the approximation. $b_{ijk}(\mathbf{X})$ are unknown coefficients and are determined by imposing the reproducing conditions (Chen *et al*. 1996). The *n*-th order reproducing conditions are the conditions such that the approximation can reproduce polynomials up to *n*-th order and can be expressed as

$$\sum_{I=1}^{NP}\Psi_I(\mathbf{X})X_{1I}^iX_{2I}^jX_{3I}^k=X_1^iX_2^jX_3^k \qquad i+j+k=0,\cdots,n \tag{9}$$

In matrix notation, the following system equation can be obtained after the *n*-th order reproducing conditions are imposed

$$\mathbf{M}(\mathbf{X})\mathbf{b}(\mathbf{X}) = \mathbf{H}(\mathbf{0}) \tag{10}$$

with the moment matrix $\mathbf{M}(\mathbf{X})$ being defined as

$$\mathbf{M}(\mathbf{X}) = \sum_{I=1}^{NP} \mathbf{H}(\mathbf{X}-\mathbf{X}_I)\mathbf{H}^T(\mathbf{X}-\mathbf{X}_I)\Phi_a(\mathbf{X}-\mathbf{X}_I) \tag{11}$$

Therefore, the unknown coefficients $b_{ijk}(\mathbf{X})$ can be solved and the correction function $C(\mathbf{X};\mathbf{X}-\mathbf{X}_I)$ and the RK shape function $\Psi_I(\mathbf{X})$ can be obtained subsequently.

$$C(\mathbf{X};\mathbf{X}-\mathbf{X}_I) = \mathbf{H}^T(\mathbf{0})\mathbf{M}^{-1}(\mathbf{X})\mathbf{H}(\mathbf{X}-\mathbf{X}_I) \tag{12}$$

$$\Psi_I(\mathbf{X}) = \mathbf{H}^T(\mathbf{0})\mathbf{M}^{-1}(\mathbf{X})\mathbf{H}(\mathbf{X}-\mathbf{X}_I)\Phi_a(\mathbf{X}-\mathbf{X}_I) \tag{13}$$

Constructed with the correction function (Eq. (12)) based on the *n*-th order complete monomial basis function (Eq. (7)), the RK approximation can reproduce polynomials up to *n*-th order completely and consistently.

It should be pointed out that the RK shape function does not possess the Kronecker delta property, therefore special strategies are required to enforce essential boundary conditions. Many approaches have been developed in the past years. For instance, Belytschko *et al.* (1994) used the Lagrange multiplier method for static problems; Lu *et al*. (1994) applied a modified variational principle; Chen *et al*. (1996 and 1998c) developed a transformation method; Belytschko and Tabbara (1996) employed the point collocation method; Zhu *et al.* (1998) used a penalty method; Wagner and Liu (2000) employed a corrected collocation method; Chen *et al.* (2003) proposed a modified reproducing kernel approximation with nodal interpolation properties; and Fernandez-Mendez and Huerta (2004) introduced a coupled FEM and EFG method for essential boundary conditions. In fact, in the coupled (FEM with EFG or RKPM) algorithm, if the essential boundary is purposely discretized by finite element approximation, then the essential boundary conditions can be applied directly and this is the approach applied in this research.

2.3 Discrete equation of motion by coupled approximation

Similar to a pure finite element or meshfree approximation, the coupled approximation for the incremental displacement is expressed as

$$\Delta u_i(\mathbf{x},t) = \sum_I \tilde{\Psi}_I(\mathbf{x})\Delta d_{iI}(t) \tag{14}$$

where $\tilde{\Psi}_I(\mathbf{x})$ is the coupled shape function, $d_{iI}(t)$ is the coefficient of the approximation.

Accordingly, the coupled approximation for the incremental strain in matrix notation can be cast as

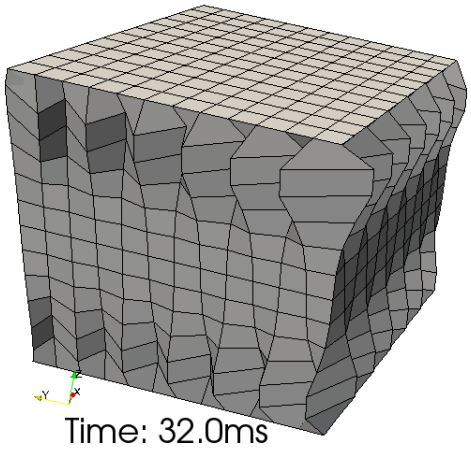

Fig. 3 Hourglass modes in cube compression without hourglass control

$$\Delta\tilde{\mathbf{e}}(\mathbf{x}) = \sum_I \tilde{\mathbf{B}}_I(\mathbf{x})\Delta\mathbf{d}_I \tag{15}$$

with the coupled gradient matrix being defined as

$$\tilde{\mathbf{B}}_I(\mathbf{x}) = \begin{bmatrix} \tilde{\Psi}_{I,1}(\mathbf{x}) & 0 & 0 \\ 0 & \tilde{\Psi}_{I,2}(\mathbf{x}) & 0 \\ 0 & 0 & \tilde{\Psi}_{I,3}(\mathbf{x}) \\ \tilde{\Psi}_{I,2}(\mathbf{x}) & \tilde{\Psi}_{I,1}(\mathbf{x}) & 0 \\ 0 & \tilde{\Psi}_{I,3}(\mathbf{x}) & \tilde{\Psi}_{I,2}(\mathbf{x}) \\ \tilde{\Psi}_{I,3}(\mathbf{x}) & 0 & \tilde{\Psi}_{I,1}(\mathbf{x}) \end{bmatrix} \tag{16}$$

where the derivatives of the coupled shape functions are calculated by

$$\tilde{\Psi}_{I,i}(\mathbf{x}) = (1-R)N_{I,i}(\mathbf{x}) + R\Psi_{I,i}(\mathbf{x}) \qquad i = 1,2,3 \tag{17}$$

The derivatives for the FE shape function are computed using the standard FEM procedure, while the derivatives of the RK shape function are

$$\begin{aligned} \Psi_{I,i}(\mathbf{x}) &= \mathbf{H}^T(\mathbf{0})\mathbf{M}^{-1}_{,i}(\mathbf{x})\mathbf{H}(\mathbf{x}-\mathbf{x}_I)\Phi_a(\mathbf{x}-\mathbf{x}_I) \\ &+ \mathbf{H}^T(\mathbf{0})\mathbf{M}^{-1}(\mathbf{x})\mathbf{H}_{,i}(\mathbf{x}-\mathbf{x}_I)\Phi_a(\mathbf{x}-\mathbf{x}_I) \qquad i = 1,2,3 \\ &+ \mathbf{H}^T(\mathbf{0})\mathbf{M}^{-1}(\mathbf{x})\mathbf{H}(\mathbf{x}-\mathbf{x}_I)\Phi_{a,i}(\mathbf{x}-\mathbf{x}_I) \end{aligned} \tag{18}$$

The spatial derivatives (in the current configuration, represented by $\mathbf{x}$) of the coupled shape function is obtained using the chain rule

$$\frac{\partial \tilde{\Psi}_I^X(\mathbf{X})}{\partial x_i} = \frac{\partial \tilde{\Psi}_I^X(\mathbf{X})}{\partial X_j}\frac{\partial X_j}{\partial x_i} = \frac{\partial \tilde{\Psi}_I^X(\mathbf{X})}{\partial X_j}F_{ji}^{-1} \qquad i,j=1,2,3 \tag{19}$$

where $\frac{\partial \tilde{\Psi}_I^X(\mathbf{X})}{\partial X_i}$ are the derivatives of the coupled shape function to the reference configuration (represented by $\mathbf{X}$). The derivatives of the FE and RK shape functions with respect to the reference configuration are calculated and saved at the very beginning of the simulation.

By substituting the coupled approximation of the incremental displacement and strain into the weak form of the equation of motion, the discrete equation for a dynamic event can be written as

$$\mathbf{M}\Delta\ddot{\mathbf{d}} = \mathbf{f}^{ext} - \mathbf{f}^{\text{int}} \tag{20}$$

where $\mathbf{M}$ is the lumped mass and the external and internal forces are integrated by

$$\mathbf{f}_I^{ext} = \int_{\Gamma_h} \tilde{\Psi}_I \mathbf{h} d\Gamma + \int_{\Omega_x} \tilde{\Psi}_I \mathbf{b} d\Omega \tag{21}$$

$$\mathbf{f}_I^{\text{int}} = \int_{\Omega_x} \tilde{\mathbf{B}}_I^T \boldsymbol{\Sigma} d\Omega \tag{22}$$

with $\mathbf{h}$ and $\mathbf{b}$ representing, respectively, the surface tractions and body forces and the Cauchy stress vector $\boldsymbol{\Sigma}$ being defined as: $\boldsymbol{\Sigma}^T = \left[\sigma_{11}\ \sigma_{22}\ \sigma_{33}\ \sigma_{12}\ \sigma_{23}\ \sigma_{31}\right]$.

2.4 Triggering criteria for coupling

The resulting FE/RK coupling approach provides an efficient algorithm that can generate a seamless evolution of particles as a response to excessive distortion being incurred in the FEM portion of the problem domain. To effectuate the evolution from FEM to RKPM, a triggering criteria needs to be selected to allow the evolution to occur automatically. The triggering criteria can be based on any combination of field or state variables that are indicative of the sort of responses causing problems to the FEM solver. For example, limits on the magnitude of pressure or velocity might be useful for conversion of areas of the model affected by shockwaves, while criteria based on limiting the magnitude of the effective plastic strain for the FEM portion of the model might be useful for metal materials. Metrics involving combinations of field and state variables computed by the constitutive laws may provide the most effective form of triggering criteria for utilizing the evolutionary coupling approach.

There are two groups of triggering criteria that might be considered. One is based on deformation, such as the deformation gradient and strain energy density criteria introduced by Lu and Chen (2002), the shear deformation, volumetric strain and unbalanced nodal distribution criteria developed by Hu *et al.* (2010) and the critical strain criteria proposed by Zhou *et al* .(1996). The other one is based on results computed by the material constitutive model such as the equivalent plastic strain and maximum shear stress criteria proposed by Batra and Lear (2004) and the material damage criteria introduced by Wu *et al.* (2013) and it is used in this research as well since the focus of this work is predicting the responses of concrete structures. The effective plastic strain provided by plasticity models can also be used as the triggering criteria. As the

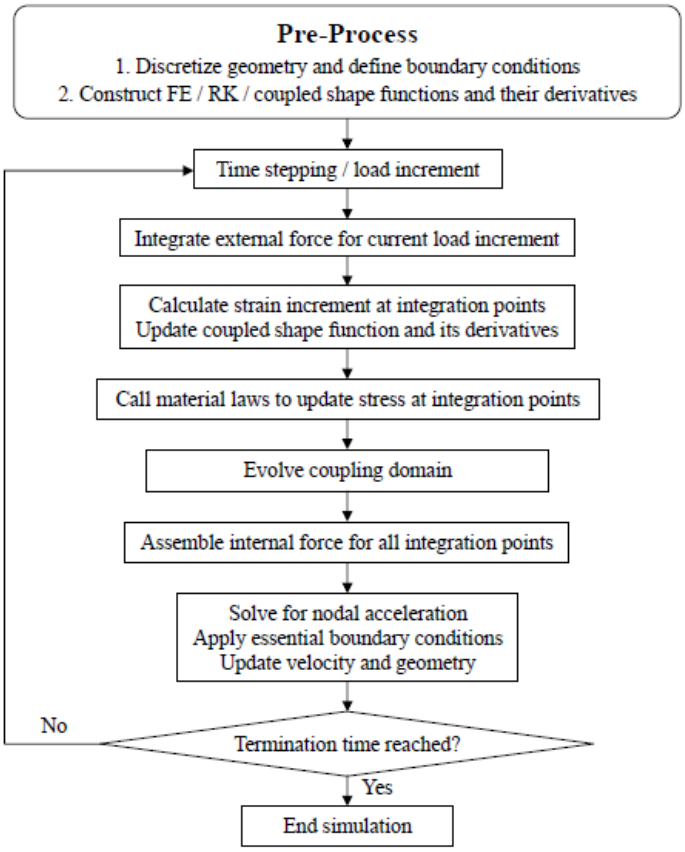

Fig. 4 Flow chart of coupled FEM/RKPM analysis

triggering criteria, the internal damage variable defined in the KCC model is discussed in detail in Section 3.

2.5 Hourglass control

As was mentioned earlier, Gauss quadrature is used as the domain integration techniqure for the weak form of the coupled approximation. Unlike SCNI, hourglass modes might occur when one-point Gauss quadrature rule is applied with hexahedral integration grids. Fig. 3 shows the sorts of hourglass modes occurred in the analysis of a concrete cube compression problem without application of any hourglass control scheme, while the weak form formulation is integrated by one-point Gauss integration with hexahedral grids. Therefore, hourglassing must be controled carefully.

In this study, hexahedral elements are used in finite element discretization and as the integration grids for meshfree discretization and only one-point integration is allowed for the material constitutive laws. Therefore, hourglass control schemes are needed to prevent the formation of hourglass modes. DYNA3D provides viscous type and stiffness type (Flanagan and Belytschko, 1981) of hourglass controls for FEM analyses. However, they are not readily applicable to meshfree calculations. The viscous type with exact volume integration was modefied

in this effort to be available for use with the coupled formulation and it is applied to all the analyses presented in this paper.

2.6 Code implementation

DYNA3D is an explicit finite element program for solving structural / continuum mechanics problems and is specially efficient in solving transient dynamic problems. The flow chart of the DYNA3D version coupled FEM / RKPM code is shown in Fig. 4.

First, the FE, RK and coupled shape functions and their derivatives are constructed and saved at the beginning of a time step. Next, the external force is integrated for the current time step, after which, the incremental strains are evaluated and stresses calculated according to the various material constitutive laws involved for the updated strain state. The coupled shape function and its derivatives are updated for the step as well using the coupling function *R* defined in the previous load step. Subsequently, the coupling function *R* is reevaluated and internal force is integrated based on the updated stress state. Finally, the acceleration is computed, essential boundary conditions are enforced and velocity and geometry (nodal coordinates) are updated and then the calculation proceeds to the next time step.

3. Constitutive modeling of concrete

The K&C concrete (KCC) model was implemented into DYNA3D in 1997 by Malvar *et al.* (1997) for application with FEM codes, particularly for one-point integrated solid elements. The KCC material model employs a three-surface plasticity formulation using an internal damage variable to compute the evolution of the plasticity surface. The KCC model has proven effective at modeling concrete and reinforced structures subjected to a variety of dynamic loadings (Crawford *et al.* 2011). It provides an ideal means to demonstrate the application of the coupled formulation.

3.1 Failure surface

The KCC model is a three-invariant plasticity model with the failure surface γ defined by interpolation between two of the three independent strength surfaces using the internal damage variable λ, which is a function of effective plastic strain. The failure surface γ is calculated by

$$\gamma\left(I_1, J_3, \lambda\right) = \begin{cases} r\left(J_3\right)\cdot\left[\eta\left(\lambda\right)\cdot\left(\Delta\sigma_m - \Delta\sigma_y\right) + \Delta\sigma_y\right] & \lambda \le \lambda_m \\ r\left(J_3\right)\cdot\left[\eta\left(\lambda\right)\cdot\left(\Delta\sigma_m - \Delta\sigma_r\right) + \Delta\sigma_r\right] & \lambda \ge \lambda_m \end{cases} \tag{23}$$

where I_1 is the first invariant of the stress tensor, which reveals volumetric responses. J_2 and J_3 are the second and third invariants of the deviatoric stress tensor and they stand for deviatoric responses. $\Delta\sigma_m$ is the maximum strength surface, $\Delta\sigma_y$ is the yield strength surface and $\Delta\sigma_r$ is the residual strength surface.

$\eta\left(\lambda\right)$ is a predefined nonlinear function that determines the interpolation of the failure surface. It ranges from zero to unity for $\lambda \le \lambda_m$ and from unity to zero when $\lambda \ge \lambda_m$ with $\eta\left(\lambda_m\right) = 1.0$. This procedure corresponds to the failure surface migrating from yield surface

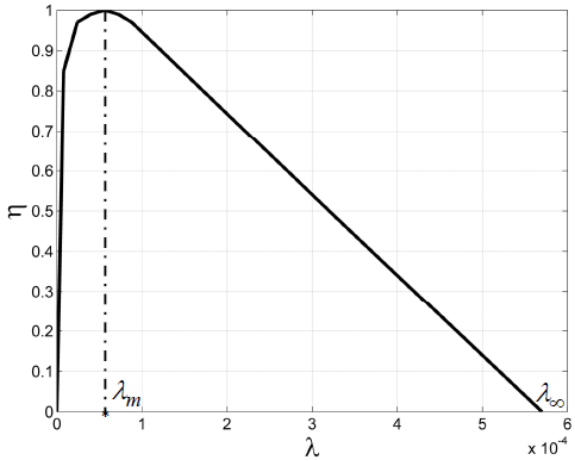

Fig. 5 Default damage function

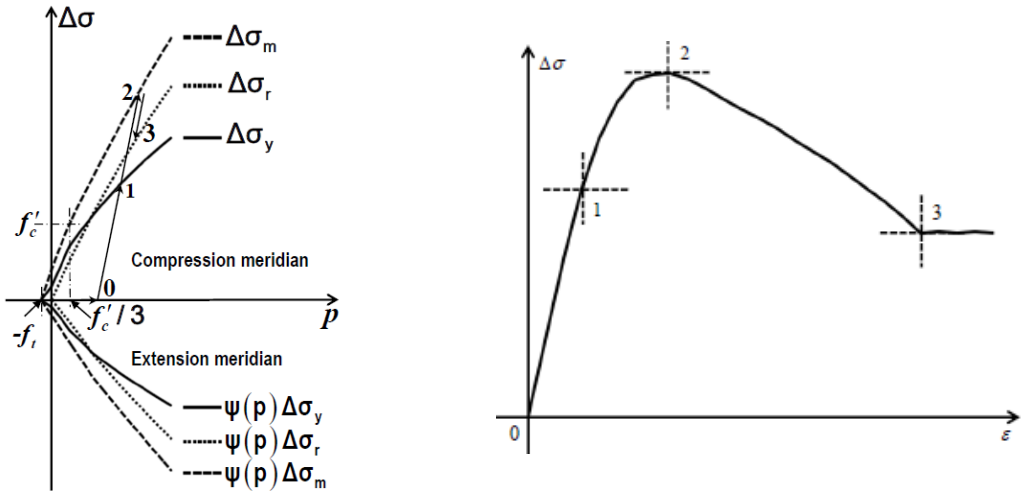

(a) Strength surfaces (b) Failure surface

Fig. 6 Strength and failure surfaces of the K&C concrete model

($\lambda = 0, \eta = 0$) to maximum surface ($\lambda = \lambda_m, \eta = 1.0$) and then to residual surface ($\lambda \geq \lambda_\infty, \eta = 0$). Strain hardening and softening behaviors are efficiently modeled by formulating the failure surface in Eq. (23). The $\eta(\lambda)$ damage function enables the KCC model to reproduce hardening until the maximum surface $\Delta\sigma_m$ is reached where the failure surface is interpolated between the yield and maximum surface ($\lambda \in [0, \lambda_m]$) and then softening until the residual surface $\Delta\sigma_r$ is reached where the failure surface is interpolated between the maximum and residual surface ($\lambda \in [\lambda_m, \infty]$). The default damage function (i.e., (λ, η) pairs) for the KCC model's generic concrete fit (Crawford *et al.* 2011) is shown in Fig. 5.

As defined in Eq. (23), the failure surface γ is a function of the third invariant J_3, via the function, r, which takes the form of the formulation proposed by William and Warnke (Chen 1982). By using this function, the brittle-ductile transition for concrete from low confinement to

high confinement can be effectively modeled.

3.2 Strength surfaces

Concrete is a pressure dependent material, therefore, its strength surfaces are defined as functions of pressure. In the KCC model, a simple function is used to express the effect of pressure ($p = -I_1 / 3$) in the strength surfaces (shown in Fig. 6(a)). Each of the strength surface is defined by three parameters a_{0i}, a_{1i} and a_{2i} (therefore, 9 parameters total for the three surfaces and they are calibrated from test data). Denoting the strength surfaces by $\Delta\sigma_i$ and they can be expressed as

$$\Delta\sigma_i = a_{0i} + \frac{p}{a_{1i} + a_{2i} \cdot p} \tag{24}$$

i stands for m, y and r, corresponding to maximum, yield and residual surface respectively.

Fig. 6(b) shows an illustration of a typical axial stress difference (i.e., failure surface) versus net axial strain response for a concrete specimen subjected to triaxial compression (TXC) loading. Stress difference is defined by total stress minus confinement pressure and net axial strain is defined as total axial strain minus the axial strain induced by confinement pressure. Subsequent to hydrostatical loading (Point 0), sample behaves linearly up to roughly 35-65% of its peak strength (Point 0 to Point 1) and then strain hardening occurs until its peak strength (Point 2) is reached. Afterwards, strain-softening is observed until it reaches the residual strength whose value depends on the level of confinement (Point 3). The figure suggests that certain confinement exists in the test since otherwise the residual strength would be zero.

3.3 Damage evolution and triggering

The yield function of the KCC model is defined as (Malvar *et al.* 1997)

$$f\left(I_1, J_2, J_3, \lambda\right) = \sqrt{3J_2} - \gamma\left(I_1, J_3, \lambda\right) \tag{25}$$

and the flow potential function is defined as

$$g\left(I_1, J_2, J_3, \lambda\right) = \sqrt{3J_2} - \omega\gamma\left(I_1, J_3, \lambda\right) \tag{26}$$

where ω is the parameter of associativity (0.0 for non-associative and 1.0 for full associative).

The internal damage variable γ is accumulated as a function of the effective plastic strain using primarily two damage accumulation parameters: b_1 and b_2 (calibrated from test data), where b_1 controls compressive and b_2 governs tensile damage evolution, respectively. From the flow rule and the yield function, the increment of the internal damage λ can be derived as

$$d\lambda = h\left(\boldsymbol{\sigma}\right)\sqrt{1 + 2\left(\frac{\omega\gamma_{,p}}{3}\right)^2}\, d\mu \tag{27}$$

where $d\mu$ is the consistency parameter of plasticity. The hardening parameter $h(\boldsymbol{\sigma})$ is defined as

$$h(\boldsymbol{\sigma}) = \begin{cases} \dfrac{1}{r_f\left(1+\frac{p}{r_f f_t}\right)^{b_1}} & p \geq 0, \textit{compression} \\ \dfrac{1}{r_f\left(1+\frac{p}{r_f f_t}\right)^{b_2}} & p < 0, \textit{tension} \end{cases} \tag{28}$$

Here, strain rate effect is enhanced through inputting a dynamic increasing factor (DIF) curve in the KCC model and r_f is the DIF at the current strain rate interpolated from the curve. f_t is the tensile strength of the concrete. Finally, the internal damage λ can be updated as

$$\lambda^{n+1} = \lambda^n + d\lambda \tag{29}$$

The internal damage λ provides a straightforward and simple means to evaluate the deformation status of a material point for use in triggering the evolution from FEM to RKPM for concrete materials in the coupled formulation. For simplicity, a normalized form of the damage variable is employed

$$\delta = 2\lambda / (\lambda + \lambda_m) \tag{30}$$

Here, λ_m is an input parameter which satisfies $\eta(\lambda_m) = 1.0$. Therefore, δ ranges from 0.0 (pre-yielding), to 1.0 (indicating that the maximum strength of the material has been reached) and then to 2.0 when the material has completely softened to the residual strength surface and no longer has any cohesion. Since the focus of the current research is the response of concrete, this variable is used as the triggering criteria. It is set to 1.995 for mesh conversion in the numerical applications shown unless a pure RKPM simulation is performed. This criteria indicates that meshfree discretization is only used in the most highly distorted regions of the model where the concrete reaches its residual strength surface.

4. Numerical results

Results are shown for the coupled formulation described above, which are from analyses of concrete structures subjected to the sorts of loads that would emanate from situations involving forms of loading, such as quasi-static, high frequency impulsive and high velocity impact. Both plain concrete and reinforced concrete structures are considered. The concrete is modeled with one-point integrated (Gauss) hexahedral elements and the KCC model; the reinforcement is modeled with beam or truss elements using a strain rate dependent isotropic elastic-plastic material model. To save computational cost, a normalized support size of 1.01 is used in all the examples for meshfree approximation. The hourglass control technique described in Section 2.5 is applied in all the analyses, otherwise, unphysical responses will be obtained or the simulation will be terminated prematurely due to hourglass modes.

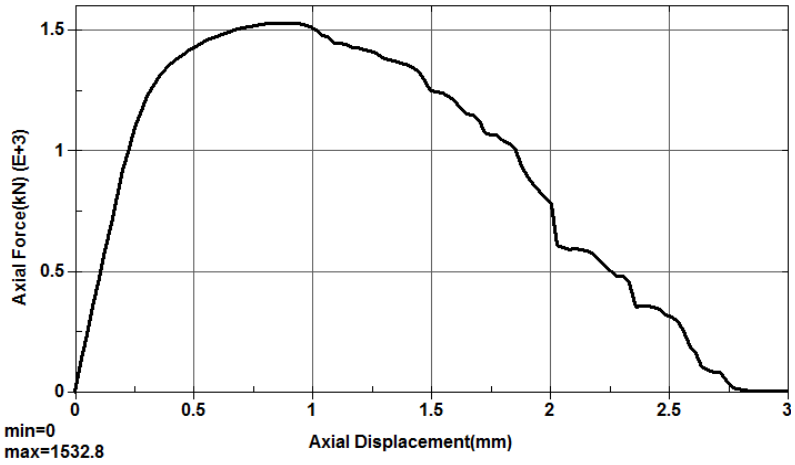

Fig. 7 Load – deflection curve for cube compression

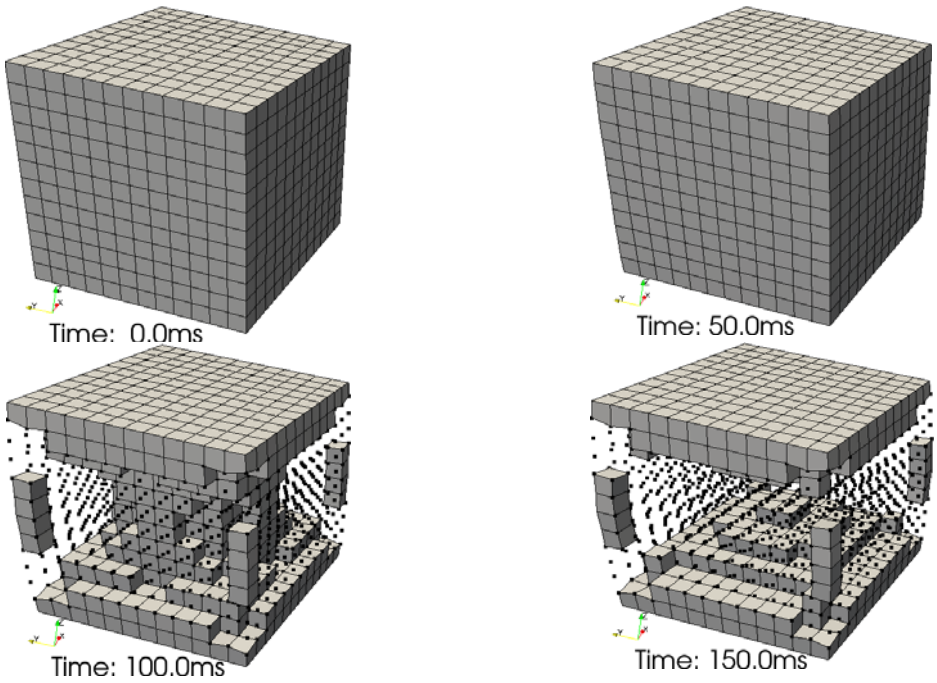

Fig. 8 Mesh advance during cube compre ssion

4.1 Unconfined uniaxial compression of plain concrete cube

A plain concrete cube is used to simulate the response obtained in a quasi-static unconfined uniaxial compression (UUC) test. The cube has a side length of 150 mm and the compressive strength of the concrete is 39.9 MPa. The bottom of the cube is fixed and the top is laterally constrained and pushed downward axially with a velocity of 25.4 mm/sec. Strain rate effects are ignored since this is a quasi-static test.

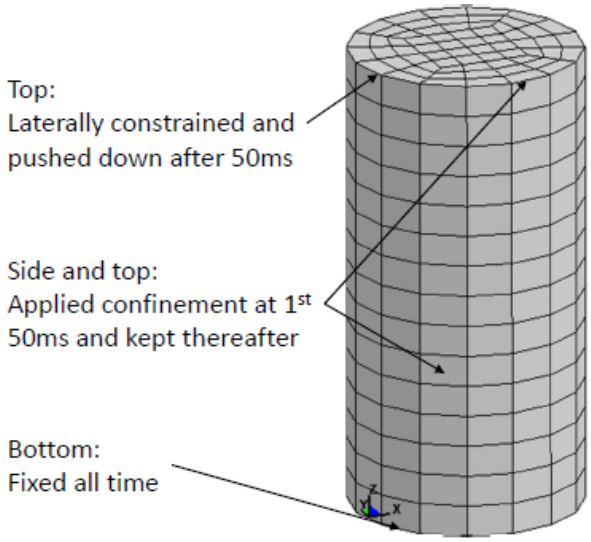

Fig. 9 Model of triaxial compression and boundary conditions

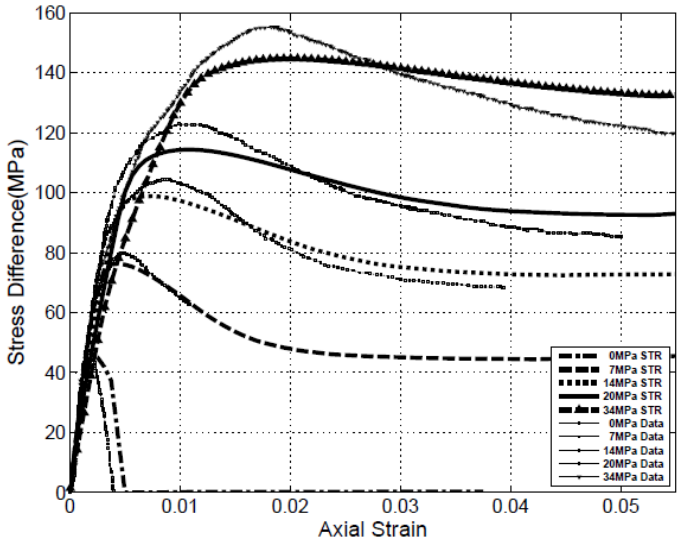

Fig. 10 Response of triaxial compression

Fig. 7 shows the axial load – deflection curve for the UUC test, where positive represents compression. It is seen that the yielding, hardening (up to peak) and post-peak softening behaviors of the concrete material are properly captured by the model. The changes in mesh as the compression is increased, that are depicted in Fig. 8 indicate the extent of severe damage since the mesh conversion is triggered by damage. In the figure, the dots represent meshfree particles and the elements (i.e., solids) represent the FEM portion of the model. It may be observed that as time goes on (i.e., compression increases), more and more regions are converted to meshfree, which indicates that the triggering mechanism works properly. In addition, the CPU cost due to the usage of meshfree approximation is increased about 120% (were pure FE approximation used).

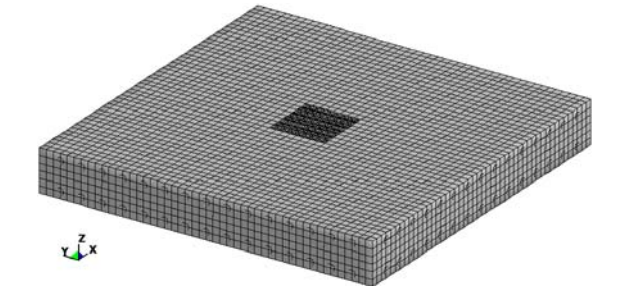

(a) Slab

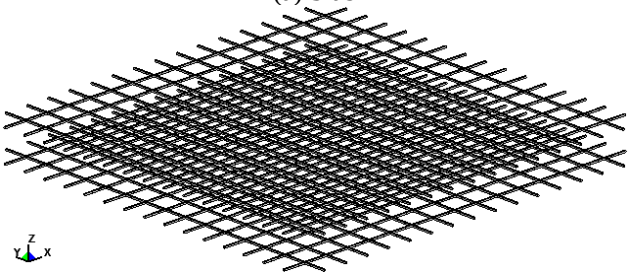

(b) Rebar

Fig. 11 Reinforced concrete slab subjected to impulsive load

4.2 Triaxial compression (TXC) of plain concrete cylinder

In this study, a plain concrete cylinder with diameter of 152.4 mm and height of 304.8 mm is used, which is shown in Fig. 9. The compressive stregnth of the concrete is 45.4 MPa. The bottom of the cylinder is fixed and the top is laterally constrained and pushed downward axially with a velocity of 76.2 mm/sec after confinement pressure is applied in the first 50 ms. Strain rate effects are not enforced since this is a quasi-static test. The simulations presented in this section are performed using only RKPM since the damage in most of these TXC tests (except the non-confined case) are very low due to the confinement.

The net axial strain – axial stress difference relationships for the TXC tests with various confinement pressures are presented in Fig. 10. The axial strain is defined as the axial displacement at the top surface divided by its original height and the net axial strain is the total axial strain minus the axial strain induced by the confinement pressure. The axial stress is calculated by the applied force divided by its original cross-sectional area and the axial stress difference is computed as the axial stress minus the confinement pressure. “STR” on the legend stands for numerical results and “Data” represents test results (Crawford *et al.* 2011). Overall, the numerical results match test data well. The yielding, hardening (up to peak) and post-peak softening behaviors of concrete are clearly simulated by the model and the brittle-ductile transition with increasing confinement is realized as well.

4.3 Reinforced concrete slab subjected to impulsive load

In this problem, as shown in Fig. 11, a 1219.2 mm by 1219.2 mm by 152.4 mm steel reinforced concrete (RC) slab is subjected to high frequency triangular impulsive loads over its central region (of 203.2 mm by 203.2 mm area, the black region in Fig. 11a). The slab is reinforced by #8 rebar

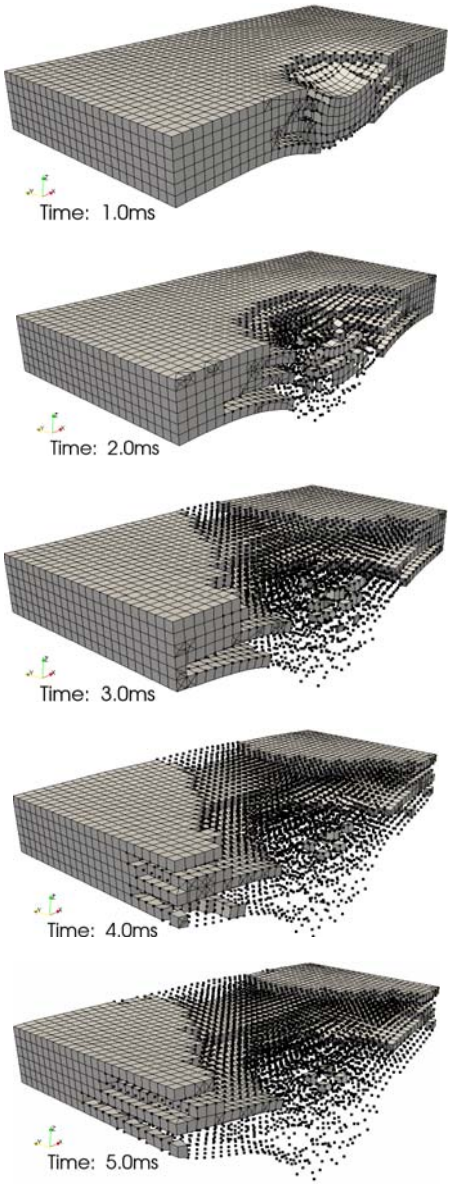

Fig. 12 Damage evolution / mesh advance in RC slab (rebar not shown)

(diameter of 25.4 mm, ASTM Grade 60 steel) at a space of 76.2 mm on center each way on each face, as shown in Fig. 11b. The peak pressure of the load is 345 MPa and its duration is 1.0 msec The concrete has an unconfined compressive strength of 34.5 MPa and the edges of the slab are clamped.

The damage evolution / mesh advance (note that mesh converion occurs when damage reaches 1.995) is shown in Fig. 12 up to 5.0 ms. For clarity, only half of the slab is plotted and rebar is not shown. It is seen that more and more of the FE mesh is converted to meshfree particles as the

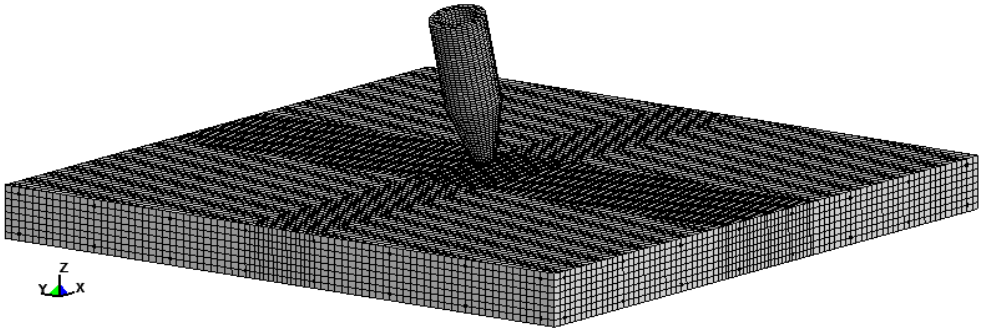

(a) Isometric view

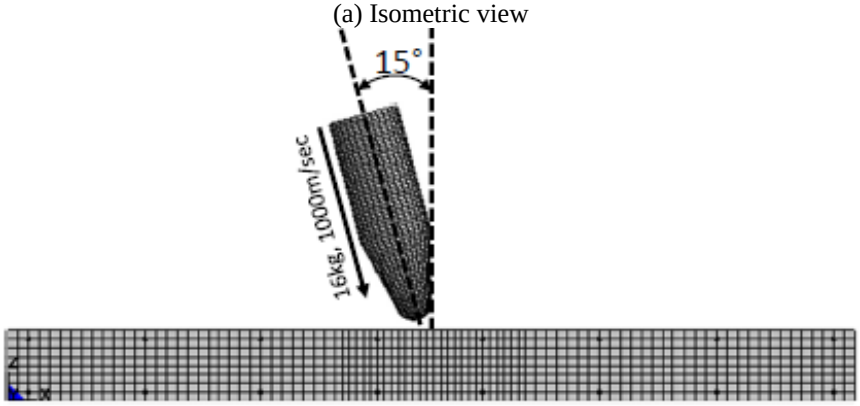

(b) Side view

Fig. 13 Model of high velocity impact

simulation continues; and cracking and separation of the slab along its tension side is apparent. These observations imply that the triggering algorithm works properly and that the fragmentation of the concrete material can be well simulated.

4.4 High velocity penetration on RC slab

In this analysis, a 1219.2 mm by 1219.2 mm by 101.6 mm steel reinforced concrete (RC) slab is impacted by a big projectile shaped fragment striking its central region, as shown in Fig. 13. The slab is reinforced by #6 rebar (diameter of 19 mm, ASTM Grade 60 steel) at a space of 152.4 mm on center each way on each face. The fragment has a mass of 16 kg and runs at 1000 m/sec (at 15° to the vertical line, Fig. 13) towards the center of the slab and it is modeled by elastic material. The interaction between the fragment and the slab is defined through sliding with separation and friction contact. The concrete has an unconfined compressive strength of 41.4 MPa and the edges of the slab are clamped.

Fig. 14 shows the damage evolution / mesh advance (occurs when damage reaches 1.995) in this high velocity impact preblem. Again, for clarity, only half of the slab is plotted and rebar is not shown. It is observed that the fragment penetrates through the slab and the slab is broken into small pieces at the impact region. These results once again shows that the coupled formulation is able to capture fragmentation of concrete structures. Compared with pure FEM simulation, tremendous CPU cost increasing (400%) was found in this simulation.

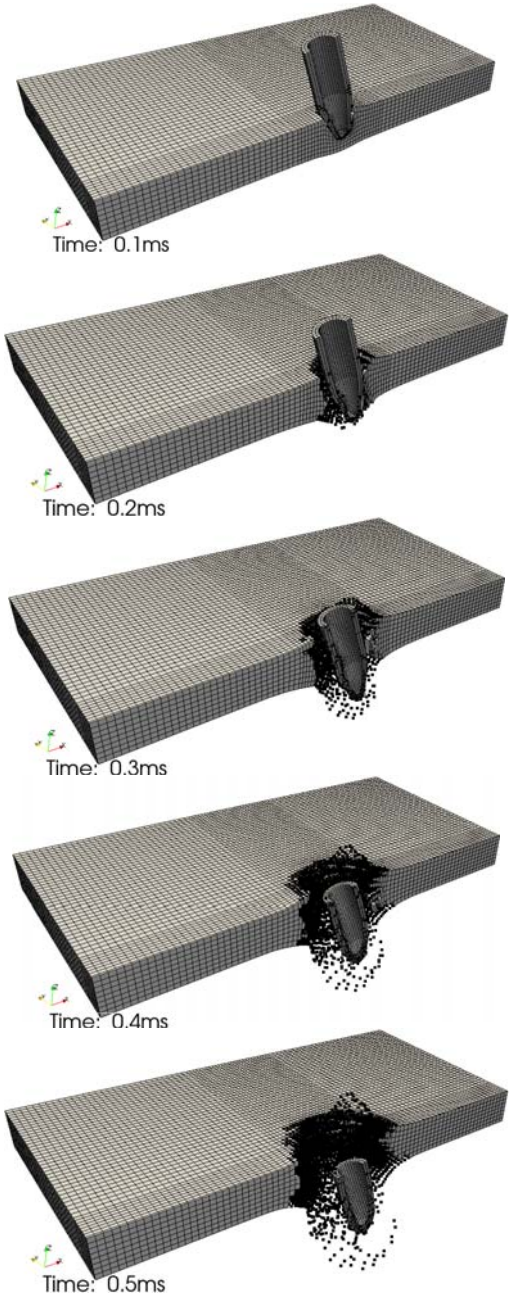

Fig. 14 Mesh advance in high velocity impact problem

5. Conclusions

An evolutionarily coupled finite element – reproducing kernel (FE/RK) formulation was implemented under the framework of DYNA3D. The coupling scheme allows automatic conversion from finite element discretization to meshfree discretization when the triggering

criteria is satisfied. In this coupling approach, FE and RK shape functions are coupled through a linear coupling function so that a smooth transition between finite element approximation and meshfree approximation is obtained.

Gauss integration is used for the finite element domain integration (i.e., in DYNA3D). To minimize computational operations when mesh conversion is performed, Gauss integration (with the integration cells exactly same as the elements used in finite element discretization) is also applied for the domain integration of meshfree discretization. This greatly facilitates the conversion process since the state variables transition is not required when finite element approximation is converted to the meshfree approximation because state variables are still stored at the same integration points rather than nodal points for the meshfree discretization. Thus, the efficiency of the scheme is assured.

To more effectively model the fragmentation phenomena associated with concrete structures stroke by high velocity projectiles, the finite element version KCC model was modified to work with the meshfree formulation and hence, the coupled approximation. The internal damage variable defined by the KCC model was chosen as the triggering criteria for the coupled approach when it is employed in analyzing the responses of concrete structures subjected to extreme loads.

Numerical results from quasi-static tests show that the basic behaviors of concrete are captured properly by the coupled formulation with the KCC model. Analyses of blast effects and impact loads show that fragmentation of concrete structures can be captured by the coupled FE/RK formulation.

References

Bardenhagen, S.G. and Kober, E.M. (2004), "The meneralized interpolation material point method", *Comput. Modeling Eng. Sci.*, **5**(6), 477-496.

Batra, R.C. and Lear, M.H. (2004), "Simulation of brittle and ductile fracture in an impact loaded prenotched plate", *Int. J. Fracture*, **126**(2), 179-203.

Belytschko, T. and Tabbara, M. (1996), "Dynamic fracture using element free Galerkin methods", *Int. J. Numer. Meth. Eng.*, **39**(6), 923-938.

Belytschko, T., Lu, Y.Y. and Gu, L. (1994), "Element-free Galerkin methods", *Int. J. Numer. Meth. Eng.*, **37**(2), 229-256.

Belytschko, T., Lu, Y.Y. and Gu, L. (1995), "Element-free Galerkin methods for static and dynamic fracture0", *Int. J. Solids Struct*., **32**(17-18), 2547-2570.

Chen, J.S. and Wang, D. (2006), "A constrained reproducing kernel particle formulation for shear deformable shell in Cartesian coordinates", *Int. J. Numer. Meth. Eng.*, **68**(2), 151-172.

Chen, J.S. and Wu, Y. (2007), "Stability in Lagrangian and semi-Lagrangian reproducing kernel discretizations using nodal integration in nonlinear solid mechanics", *Compu.Meth. Appl. Mech. Eng.*, (Eds. V. M. A. Leitao, C.J.S. Alves, C. A. Duarte), Springer, 55-77

Chen, J.S., Crawford, J.E. and Wu, Y. (2006), "Development of meshfree methods for fragment impact problems", TR 06 58.1, Karagozian & Case, Burbank, CA.

Chen, J.S., Han, W., You, Y. and Meng, X. (2003), "A reproducing kernel method with nodal interpolation property", *Int. J. Numer. Meth. Eng.*, **56**, 935-960.

Chen, J.S., Pan, C. and Wu, C.T. (1998c), "Application of reproducing kernel particle method to large deformation contact analysis of elastomers", *Rubber Chem. Tech.*, **71**, 191-213.

Chen, J.S., Pan, C. and Wu, C.T. (1998b), "Large deformation analysis of rubber based on a reproducing kernel particle method", *Comput. Mech*., **22**, 289-307.

Chen, J.S., Pan, C., Roque, C.M.O.L. and Wang, H. (1998a), "A Lagrangian reproducing kernel particle

method for metal forming analysis", *Comput. Mech.*, **22**, 289-307.
Chen, J.S., Pan, C., Wu, C.T. and Liu, W.K. (1996), "Reproducing kernel particle methods for large deformation analysis of nonlinear structures", *Compu.Meth. Appl. Mech. Eng.*, **139**, 195-227
Chen, J.S., Wu, C.T., Chi, L.C. and Huck, F. (2001b), "A Lagrangian meshfree formulation for geotechnical material", *J. Eng. Mech.*, **127**, 440-449.
Chen, J.S., Wu, C.T., Yoon, S. and You, Y. (2001a), "A stabilized conforming nodal integration for Galerkin meshfree methods", *Int. J. Numer. Meth. Eng.*, **50**, 435-466, 2001.
Chen, J.S., Wu, C.T., Yoon, S. and You, Y. (2002), "Nonlinear version of stabilized conforming nodal integration for Galerkin meshfree methods", *Int. J. Numer. Meth. Eng.*, **53**, 2587-2615.
Chen, W.F. (1982), "Plasticity in Reinforced Concrete", McGraw Hill, New York
Courant, R. (1942), "Variational methods for the solution of problems of equilibrium and vibrations", Transaction of American Mathematical Society, 1-23.
Crawford, J.E., Chen, J.S., Choi, H.J. and Wu, Y. (2005), "Description of meshfree methods developed for fragment impact, penetrations and other problems", TR-05-71.1, Karagozian & Case, Burbank, CA.
Crawford, J.E., Magallanes, J.M., Lan, S. and Wu, Y. (2011), *User's manual and documentation for release III of the K&C concrete material model in LS-DYNA*, TR-11-36-1, Technical report, Karagozian & Case, Burbank, CA.
Fernandez-Mendez, S. and Huerta, A. (2004), "Imposing essential boundary conditions in mesh-free methods", *Compu.Meth. Appl. Mech. Eng.*, **193**, 1257-1275.
Flanagan, D.P. and Belytshcko, T. (1981), "A uniform strain hexahedron and quadrilateral with orthogonal hourglass control", *Int. J. Numer. Meth. Eng.*, **17**, 679-706.
Gingold, R.A. and Monaghan, J.J. (1972), "Smooth particle hydrodynamics: theory and application to non-spherical stars", Monthly Notices of the Royal Astronomical Society, **181**, 375-389.
Guan, P.C., Chen, J.S., Wu, Y., Teng, H., Gaido,s J., Hofstetter, K. and Alsaleh, M. (2009), "Semi-Lagrangian reproducing kernel formulation and application to modeling earth moving operations", *Mech. Mater.*, **41**, 670-683.
Guan, P.C., Chi, S.W., Chen, J.S., Slawson, T.R. and Roth, M.J. (2011), "Semi-Lagrangian reproducing kernel particle method for fragment-impact problems", *Int. J. Impact Eng.*, **38**, 1033-1047.
Guo, Y., Wu, C.T., Botkin, M.E. and Wang, H.P. (2004), "Coupled FEM/Meshfree shear-deformable shells for nonlinear analysis of shell structures", *Proceedings of WCCM VI in conjunction with APCOM 04*, September, Beijing, China.
Hu, W., Wu, C.T. and Saito, K. (2010), "LS-DYNA meshfree interactive adaptivity and its application", *11th international LS-DYNA Users Conference*, Detroit, MI.
Lin, J.I. (2005), *DYNA3D: a nonlinear, explicit, three-dimensional finite element code for solid and structural mechanics*, User Manual, UCRL-MA-107254, Methods Development Group, Lawrence Livermore National Laboratory.
Liu, W.K., Jun, S. and Zhang, Y.F. (1995), "Reproducing kernel particle methods", *Int. J. Numer. Meth. Fluids*, **20**, 1081-1106.
Liu, W.K., Jun, S., Sihling, D.T., Chen, Y. and Hao, W. (1997), "Multiresolution reproducing kernel particle method for computational fluid dynamics", *Int. J. Numer. Meth. Fluids*, **24**(12), 1391-1415.
Lu, H. and Chen, J.S. (2002), "Adaptive meshfree particle method", *Lecture Notes Comput. Sci. Eng.*, **26**, 251-267.
Lu. Y.Y., Belytschko, T. and Gu, L. (1994), "A new implementation of the element free galerkin methods", *Compu. Meth. Appl. Mech. Eng.*, **113**, 397-414.
Malvar, L.J., Crawford, J.E., Wesevich, J.W. and Simons, D. (1997), "A plasticity concrete material model for DYNA3D", *Int. J. Impact Eng.*, **19**, 847-873.
Monaghan, J.J. (1988), "An introduction to SPH", *Comput. Physic. Commun.*, **48**, 89-96.
Puso, M.A., Chen, J.S., Zywicz, E. and Elmer, W. (2008), "Meshfree and finite element nodal integration method", *Int. J. Numer. Meth. Eng.*, **74**, 416-446.
Rabczuk, T. and Eibl, J. (2003), "Simulation of high velocity concrete fragmentation using SPH/MLSPH", *Int. J. Numer. Meth. Eng.*, **56**, 1421-1444.

Wagner, G.J. and Liu, W.K. (2000), "Application of essential boundary conditions in mesh-free methods: a corrected collocation method", *Int. J. Numer. Meth. Eng.*, **47**, 1367-1379.
Wang, D. and Chen, J.S. (2008), "A Hermite reproducing kernel approximation for thin plate analysis with sub-domain stabilized conforming integration", *Int. J. Numer. Meth. Eng.*, **74**, 368-390
Wang, D. and Lin, Z. (2011), "Dispersion and transient analyses of Hermite reproducing kernel Galerkin meshfree method with sub-domain stabilized conforming integration for thin beam and plate structures", *Comput. Mech.*, **48**, 47-63.
Wang, D. and Sun, Y. (2011), "A Galerkin meshfree formulation with stabilized conforming nodal integration for geometrically nonlinear analysis of shear deformable plates", *Int. J. Comput. Meth.*, **8**, 685-703.
Wang, D. and Wu, Y. (2008), "An efficient Galerkin meshfree analysis of shear deformable cylindrical panels", *Interact. Multiscale Mech.*, **1**, 339-355.
Wang, D. and Chen, J.S. (2004), "Locking-free stabilized conforming nodal integration for meshfree Mindlin-Reissner plate formulation", *comput. Meth. Appl. Mech. Eng.*, **193**, 1065-1083.
Wang, D. and Chen, J.S. (2006), "A locking-free meshfree curved beam formulation with the stabilized conforming nodal integration", *Comput. Mech.*, **39**(1), 83-90.
Wang, D., Li, Z., Li, L. and Wu, Y. (2011), "Three dimensional efficient meshfree simulation of large deformation failure evolution in soil medium", *Sic. China-Tech. Sci*., **54**, 573-580.
Wang, H.P., Wu, C.T., Botkin, M. and Guo, Y. (2009), "A coupled meshfree/finite element method for automotive crashworthiness simulations", *Int. J. Impact Eng.*, **36**(10-11), 1210-1222.
Wu, Y. (2005) "A stabilized semi-Lagrangian Galerkin meshfree formulation for extremely large deformation analysis", Ph.D. Dissertation, UCLA.
Wu, Y., Magallanes, J.M., Choi, H.J. and Crawford, J.E. (2013), "An evolutionarily coupled finite element - meshfree formulation for modeling concrete behaviors under blast and impact loadings", *ASCE J. Eng. Mech*., **139**(4), 525-536.
Zhou, M., Ravichandran, G. and Rosakis, A.J. (1996), "Dynamically propagating shear bands in impact-loaded prenotched plates – 2. Numerical Simulations", *J. Mech. Physic Solid*, **44**(6), 1007-1032.
Zhu, T., Zhang, J.D. and Atluri, S.N. (1998), "A meshless local boundary integral equation (LBIE) method for solving nonlinear problems", *Comput. Mech.*, **22**, 174-186.